Geophysical Prospecting

EAGE EUROPEAN ASSOCIATION OF GEOSCIENTISTS & ENGINEERS

Geophysical Prospecting, 2010, **58**, 925–938 doi: 10.1111/j.1365-2478.2010.00865.x

Multifocusing revisited - inhomogeneous media and curved interfaces*

Evgeny Landa[1], Shemer Keydar[2] and Tijmen Jan Moser[3†]

[1]*OPERA, Applied Geophysical Research Group, Avenue de l'Université, BP 1155, 64013 Pau Cedex, France* [2]*Geophysical Institute of Israel, PO Box 182, Lod 71100, Israel, and* [3]*Van Alkemadelaan 550A, 2597 AV Den Haag, the Netherlands*

Received October 2008, revision accepted December 2009

ABSTRACT

We review the multifocusing method for traveltime moveout approximation of multicoverage seismic data. Multifocusing constructs the moveout based on two notional spherical waves at each source and receiver point, respectively. These two waves are mutually related by a focusing quantity. We clarify the role of this focusing quantity and emphasize that it is a function of the source and receiver location, rather than a fixed parameter for a given multicoverage gather. The focusing function can be designed to make the traveltime moveout exact in certain generic cases that have practical importance in seismic processing and interpretation. The case of a plane dipping reflector (planar multifocusing) has been the subject of all publications so far. We show that the focusing function can be generalized to other surfaces, most importantly to the spherical reflector (spherical multifocusing). At the same time, the generalization implies a simplification of the multifocusing method. The exact traveltime moveout on spherical surfaces is a very versatile and robust formula, which is valid for a wide range of offsets and locations of source and receiver, even on rugged topography. In two-dimensional surveys, it depends on the same three parameters that are commonly used in planar multifocusing and the common-reflection surface (CRS) stack method: the radii of curvature of the normal and normal-incidence-point waves and the emergence angle. In three dimensions the exact traveltime moveout on spherical surfaces depends on only one additional parameter, the inclination of the plane containing the source, receiver and reflection point. Comparison of the planar and spherical multifocusing with the CRS moveout expression for a range of reflectors with increasing curvature shows that the planar multifocusing can be remarkably accurate but the CRS becomes increasingly inaccurate. This can be attributed to the fact that the CRS formula is based on a Taylor expansion, whereas the multifocusing formulae are double-square root formulae. As a result, planar and spherical multifocusing are better suited to model the moveout of diffracted waves.

Key words: Multifocusing method, Moveout formulae, Subsurface imaging.

INTRODUCTION

Even with the advent of prestack depth imaging, time-domain imaging techniques remain important for many reasons. A high-quality time imaging can provide a basis for interpretation in the processing sequence and often a useful one, even in case of poor data quality or strong structural complexity. Time imaging is basically model independent and does not require estimation or construction of a velocity model of the subsurface which is a crucial problem of seismic imaging. In the process of constructing a time image, useful additional products such as an root-mean-square (RMS) velocity and several important wavefield attributes can be obtained. Time-domain

*This paper is based on extended abstract U026 presented at the 71st EAGE Conference & Exhibition Incorporating SPE EUROPEC 2009, 8–11 June 2009 in Amsterdam, the Netherlands.

†E-mail: mosertj@gmail.com

stacking plays a key role in several model-independent imaging techniques (Hubral 1999). For these reasons, improving the quality of time-domain stacked sections remains the focus of intensive research, in particular towards improving the accuracy of the normal moveout (NMO) correction (Taner and Koehler 1969; Malovichko 1978; May and Straley 1979; Sword 1987; de Bazelaire 1988; Castle 1994; Alkhalifah and Tsvankin 1995; Causse, Hangen and Rommel 2000; Causse 2002; Taner *et al.* 2007). Historically, efforts to obtain an optimal stack have concentrated on single common-midpoint (CMP) gathers, with attempts to improve on the hyperbolic moveout and several proposals for non-hyperbolic moveout. An overview is given in Landa (2007), to which we refer for many references.

For about a decade, two apparently similar techniques have been co-existing that both aim at obtaining an optimal zero-offset approximation from multicoverage data: multifocusing (MF) (Gelchinsky, Berkovitch and Keydar 1999a,b) and the common-reflection surface stack (CRS) (Jäger *et al.* 2001). Both methods consider a collection of traces whose sources and receivers are in a vicinity of the imaging trace (a supergather), rather than a single CMP gather at a time. They are therefore referred to as non-CMP oriented methods (Landa 2007; Tygel and Santos 2007). One of the distinct advantages of non-CMP oriented methods is that they obtain stacked sections with typically a much higher signal-to-noise ratio and thus resolution and interpretability, due to the higher number of traces entering the stack. MF and CRS have additional advantages such as estimation of the RMS (root-mean-square) velocity, which can be directly used in prestack time migration, better imaging of curved interfaces due to estimation of the radius of curvature of the normal wave (R_N, see below, which is connected to the curvature of reflection interfaces), taking into account rugged surface topography, better implementation of the AVO procedure in time domain etc. (for more details see Landa 2007).

Although both techniques, MF and CRS, may have different implementations, both attempt to find, for each CMP location and each time sample, a traveltime surface that optimally fits the moveout across a collection of neighbouring CMP gathers. For both techniques, in two dimensions, the traveltime surface is parametrized by three parameters: the radii of the normal (N) and normal-incidence-point (NIP) waves, R_N and R_{NIP} respectively and the emergence angle, β (Gelchinsky *et al.* 1999a,b; Mann *et al.* 1999; Jäger *et al.* 2001; in the first reference R_N is denoted as R_{CEE} (for common-evolute-element) and R_{NIP} as R_{CRE} (for common-reflection-element)).

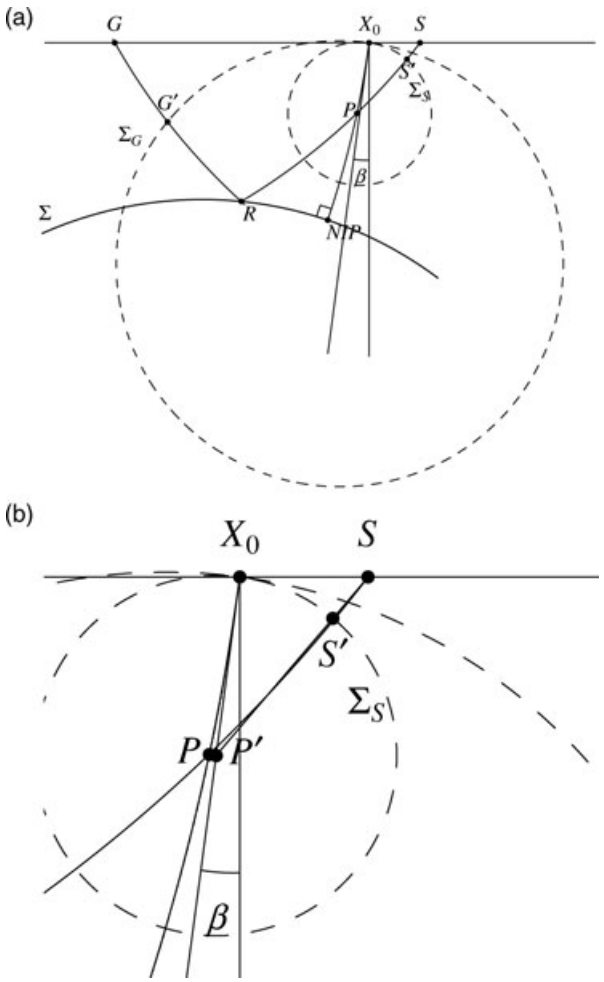

Figure 1 a) Geometrical construction of multifocusing. The multifocusing moveout is constructed as correction on two spherical wavefronts Σ_S and Σ_G. b) Law of cosines for the basic derivation of multifocusing moveout.

The MF/CRS parameters β, R_N and R_{NIP} have a clear physical interpretation, which allows a direct application in structural interpretation and velocity model building/inversion. The NIP wave, originating from a point source at a subsurface reflector, has a radius of curvature that depends on the propagation distance to the acquisition surface and hence on the depth of the reflector. The normal wave is initiated at the reflector as a parallel wave (as in the exploding reflector concept) and contains information on its curvature. The emergence angle contains information on the reflector dip (see Figs 1 and 2 for an illustration of β, R_N and R_{NIP}).

Two comparative studies of multifocusing and the common-reflection surface stack have been reported (Tygel, Santos and Schleicher 1999; Tygel and Santos 2007). The

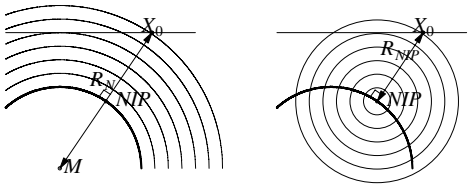

Figure 2 Geometrical meaning of N- and NIP-waves. The N-wave radius of curvature R_N is related to reflector curvature, the NIP-wave radius of curvature R_{NIP} to its depth.

general conclusion of these studies is that MF and CRS are very similar in accuracy and computational requirements and conceptual differences have not been put forward. No important advantages of one method with respect to the other have been known until now. The common-reflection surface stack method has been widely published and discussed by several authors and in numerous papers (Jäger *et al.* 2001; Eisenberg-Klein *et al.* 2008). There is a general agreement that CRS is very simple to implement and that it allows for an easy generalization to three dimensions. At the same time multifocusing has not yet received wide attention (Gelchinsky *et al.* 1999a,b; Berkovitch, Belfer and Landa 2008).

This paper serves several purposes. First, it gives an updated review of the multifocusing method. It discusses a special case commonly used until now (planar multifocusing) and introduces spherical multifocusing, which considerably extends the potential and meaning of multifocusing. Second, we investigate the differences between multifocusing and the common-reflection surface stack method and explore the potential and range of validity of both.

MULTIFOCUSING

We start by reviewing some well-known material useful for subsequent sections. We consider the ray diagram in Fig. 1(a). A central (normal) ray starts at the central point X_0 at an angle β with the vertical, hits the reflector Σ at the normal-incidence point *NIP* and turns back to X_0. Its reflection traveltime is denoted by T_0. We also consider a neighbouring (paraxial) ray from the source point S, reflecting on Σ at R and emerging at the receiver G. The purpose of multifocusing is to express the traveltime S-R-G in terms of T_0 and two corrections at S and G. This is done by considering a notional wave, which initially has the wavefront Σ_S, then implodes and focuses at the intersection point P of the normal and paraxial ray and emerges at X_0 as the wavefront Σ_G. To apply the corrections at S and G, we make the assumptions that the near-surface velocity v_0 is known and constant and that the wavefronts Σ_S and Σ_G can be locally approximated by spherical surfaces. Under these assumptions, the corrections can be approximated by straight ray segments SS' and GG' and derived from simple trigonometry. We show this in Fig. 1(b) for the source, noting that thanks to reciprocity of S and G, the same applies for G. In Fig. 1(b) the normal ray is rectified along its tangent at X_0 and the point P' is chosen so that $X_0P = X_0P'$. Then in the triangle $P' - X_0 - S$ we apply the law of cosines and obtain the correction for the traveltime along SS'. The result for both S and G is a double-square root equation for the traveltime, which is expressed as follows:

$$T(S,G) = \frac{1}{v_0}\left[\sqrt{(R^+)^2 + 2R^+\Delta X^+ \sin\beta + (\Delta X^+)^2} + \sqrt{(R^-)^2 + 2R^-\Delta X^- \sin\beta + (\Delta X^-)^2}\right] \quad (1)$$

where

$$\Delta X^+ = x_S - x_0,\ \Delta X^- = x_G - x_0.$$

Here, x_S, x_G and x_0 are the x-coordinates of the source S, receiver G and central CMP location X_0, R^+ and R^- are the radii of curvature of the notional wavefronts Σ_S and Σ_G, respectively. By moving the source and receiver point along the surface, the focusing point P is moved up and down along the normal ray – hence the name multifocusing. Based on dynamic ray theory, it is possible to show that the radii R^+ and R^- are related to the radii of curvature of the two fundamental wave fronts corresponding to the normal (N) and NIP wave (Hubral 1983; Gelchinsky *et al.* 1999a and Appendix A to this paper), by the following relation:

$$R^{\pm} = \frac{1 \pm \sigma}{\frac{1}{R_N} \pm \frac{\sigma}{R_{NIP}}}. \quad (2)$$

The quantity σ is related to the focusing of N- and NIP-waves and is discussed in detail below. The N- and NIP-waves have been used extensively in the literature, and their geometrical meaning is illustrated in Fig. 2. The normal wave is formed by normal rays emitted from the reflector (like in an exploding-reflector experiment) and the NIP wave is formed by a point source at the normal-incidence point *NIP* associated with the central point X_0.

Before proceeding, we make a few comments on equations (1) and (2). First, the multifocusing description for traveltime (1) leads to the following expression for multifocusing traveltime moveout relative to the central ray:

$$\Delta T(S,G) = T(S,G) - \frac{R^+ + R^-}{v_0}, \quad (3)$$

which does not explicitly depend on T_0. In our terminology, we will not rigorously distinguish between traveltime and

traveltime moveout. Second, the focusing quantity σ in equation (2) is equal to the ratio between X_0-*NIP* and *P*-*NIP* and has a clear physical meaning (Landa *et al.* 1999; Gelchinsky *et al.* 1999b). For $\sigma = 0$, $R^+ = R^- = R_N$ and the focusing point P lies on the centre of curvature of the reflector, which corresponds to the zero-offset configuration ($\Delta X^+ = \Delta X^-$). For $\sigma = \pm 1, R^{\mp} = 0$, which corresponds to the common-source and common-receiver configurations. For $\sigma = \infty, R^+ = R^- = R_{NIP}$, which corresponds to the case where P coincides with *NIP*. Third, we note that the double-square root expression for multifocusing moveout (1) is an approximation for a constant near-surface velocity v_0 and locally spherical wavefronts Σ_S and Σ_G. For the general case of a curved reflector and inhomogeneous overburden, (1) is therefore a short-offset approximation around the zero-offset central ray. This is not a principal restriction, as the same construction involving a central and paraxial ray can be set up for a finite-offset central ray, although this has not been implemented in practice until now (Gelchinsky *et al.* 1999a). Finally, for a single CMP gather, the multifocusing moveout correction (3) reduces to the shifted hyperbola of de Bazelaire (1988).

So far, the above material can be found in Landa *et al.* (1999) and Gelchinsky *et al.* (1999a,b). In this paper, we further elaborate on the role of the focusing quantity σ. As it stands, the multifocusing moveout (1)–(3) is parametrized by four parameters: β, R_N, R_{NIP}, and σ. These parameters are different in nature, in the sense that β, R_N, R_{NIP} are fixed for the given set of CMP's (supergather) under investigation. As such, β, R_N and R_{NIP} can be estimated in a parameter estimation procedure, such as maximizing semblance over a range of surfaces with varying (β, R_N, R_{NIP}). However, an important but often overlooked feature of multifocusing is the fact that σ is a general undetermined function of the source and receiver location. Since σ is different for different source and receiver locations, it cannot be estimated as a fixed parameter, or it would have to be determined for each source/receiver separately (which would result in an $n + 3$-parameter search, for n source/receiver pairs). In other words: σ is a function of parameters, rather than itself a parameter.

Therefore, for the general case a focusing function $\sigma = \sigma(\beta, R_N, R_{NIP}, S, G)$ needs to be established. This is done by considering a typical Earth model, in which a σ-function can be derived, such that the multifocusing moveout becomes exact for that model (but approximate for all other models). As a result, in theory, σ can be adjusted, for each S and G independently, so that the multifocusing formula can be made exact for a wide range of moveout relations in a given model (as can be seen by inserting (2) in (1) and solving for σ). The focusing function σ then depends on the parameters defining the model. These parameters could include the depth, dip and curvature of a target reflector, or any other parameter defining the geometry and overburden velocity model. In this way, for a wide range of geometries a multifocusing moveout may be designed that is exact for that case (but approximate for all other cases). For instance, in theory, we may want to construct the multifocusing moveout over a reflector defined by a B-spline with parameters given by its support points.

In practical applications, the dependence of σ on $(\beta, R_N, R_{NIP}, S, G)$ is constructed in such a way that the multifocusing formula is exact for a common, generic case. The value and usefulness of such formulae depends on criteria such as efficiency and generality. A minimal number of parameters ensures that they can be reliably estimated in a multiparameter search procedure with a reasonable computational effort. On the other hand, the formulae need to be sufficiently general so that they are robust and accurate for cases other than they were designed for. We discuss here two generic cases: the planar and spherical approximation with a constant overburden.

PLANAR MULTIFOCUSING

In all publications of multifocusing moveout expressions until now, σ is constructed for the case of a planar dipping reflector and constant overburden. To derive the σ-function for this case, R_N is taken equal to infinity. Derivations are given in Landa *et al.* (1999) and Gelchinsky *et al.* (1999b). In Appendix A to this paper, we give a general derivation of σ based on dynamic ray theory and approximation to small reflector curvature. In Appendix B we give an alternative derivation based on a planar reflector and simple geometrical principles. For planar topography the expression for σ is:

$$\sigma = \frac{\Delta X^+ - \Delta X^-}{\Delta X^+ + \Delta X^- + 2\frac{\Delta X^+ \Delta X^-}{R_{NIP}} \sin\beta}. \tag{4}$$

We refer to the multifocusing expression (1) and (2) with the planar approximation for σ as *planar multifocusing*. We note that $R_N = \infty$ is only assumed in the derivation for σ, but that (1) and (2) can also be used for curved reflectors with $R_N < \infty$. In fact, (1) with (2) and (4) is exact for the case it is designed for (a planar reflector and constant overburden) and approximate for all other cases. Experience shows that the approximation is generally remarkably good, wherever it is a regular expression; see the numerical tests presented below (Figs 6–8). However, for large offsets, or large ΔX^- or ΔX^+,

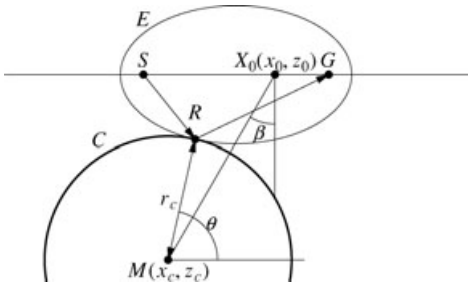

Figure 3 Spherical formula for σ, derived from the reflection traveltime between S and G on the circular reflector C (see Appendix C).

singularities appear. A three-dimensional version of the planar multifocusing has not been proposed so far.

SPHERICAL MULTIFOCUSING

If we want to generalize the planar approximation to curved reflectors, it quickly becomes clear that simple formulae for σ are available only for a few special cases. For one part, this is due to the complexity of the basic multifocusing formulae (1) and (2). For another part, it is due to the complexity of expressions for the reflection travel time themselves. A straightforward generalization of the planar multifocusing formulae (1), (2) and (4) is to consider a reflector with constant and finite R_N, R_{NIP} and β. This is the case of a spherical reflector, with a fixed radius r_c and centre of curvature (x_c, z_c) related to (β, R_N, R_{NIP}) by

$$R_N = [(x_0 - x_c)^2 + (z_0 - z_c)^2]^{1/2},$$
$$R_{NIP} = R_N - r_c, \sin\beta = (x_c - x_0)/R_N, \tag{5}$$

see Fig. 3 (compare with Fig. 2 for the meaning of R_N and R_{NIP}). Like in the case of planar multifocusing, the reflection traveltime from a source S to a receiver G depends again on the three parameters R_N, R_{NIP} and β. If the traveltime S-R-G for a general point R on the circle, given by $x = x_c + r_c \cos\theta, z = z_c + r_c \sin\theta$, is denoted by $T(\theta)$, then the specular reflection traveltime is equal to its stationary values given by $\mathrm{d}T/\mathrm{d}\theta = 0$.

The problem of reflection traveltime on a spherical reflector has a long history and is also known as Alhazen's problem (Dörrie 1965; Neumann 1998). The problem of finding the light ray from a source, reflecting on a spherical mirror and reaching a receiver point is equivalent to the circular billiard problem: given two billiard balls on a circular billiard table, to find the angle under which one has to hit one of them in order to hit the other with one bounce on the edge of the table. The same problem also appears in collision detection in computer graphics and robotics (Choi, Wang and Kim 2003). Neumann (1998) and Drexler and Gander (1998) showed that the problem leads to a quartic (fourth-order algebraic) equation. In Appendix C to this paper, we summarize the derivation from the latter reference.

The resulting equation (29) for the reflection traveltime has four complex-valued solutions in general. The two most common cases are when the source and receiver are located above a convex or concave spherical reflector (in fact, to adequately account for the concave case, a parametrization by signed reflector curvature is more convenient than R_N). In both cases, there is a single real-valued solution. Analytical expressions are available for these solutions, which we do not list here due to their algebraic complexity (see, e.g., Burnside and Panton 1960). Alternatively, the traveltime and reflection point can be found by very fast numerical algorithms, e.g., root finding on $Q(u) = 0$ (29) or on $\mathrm{d}T/\mathrm{d}\theta = 0$, or optimizing for $T(\theta)$. In either case, analytical or numerical, we have an efficient procedure that returns T as a function of $(S, G, v_0, \beta, R_N, R_{NIP})$ accurate to machine precision. For our purposes, we consider this as an exact moveout for the spherical reflector and denote it as

$$T = \Theta(S, G, v_0, \beta, R_N, R_{NIP}), \tag{6}$$

or short as $T = \Theta(S,G)$. The spherical moveout formula does not only give the reflection traveltime, but also the location of the reflection point R. Therefore, for given $(S, G, v_0, \beta, R_N, R_{NIP})$, it allows to derive the multifocusing parameters R^+ and R^- and focusing function σ. Hence, it fits in the general framework of multifocusing given by (1) and (2). In fact, it can be argued that for any general move-out expression by a double-square root, $T = \sqrt{f^+(\Delta X^+)} + \sqrt{f^-(\Delta X^-)}$, with general argument functions $f^+(\Delta X^+)$ and $f^-(\Delta X^-)$ depending on the source and receiver offsets ΔX^+ and ΔX^-, the functions f^+ and f^- must be related by a focusing mechanism (for instance, at zero-offset $\sqrt{f^+(0)} + \sqrt{f^-(0)}$ must be equal to T_0, and first- and higher-order derivatives of f^+ and f^- must be related, see Appendix A).

The spherical formula is valid for any general location of the source and receiver point S and G. Therefore, it applies without modification to general topography of the data acquisition surface. It can also be applied in other data geometries than surface seismics, e.g., in vertical seismic profiling geometries. It does not explicitly depend on a central ray and therefore applies to wide offset ranges, without singularities (appearing for large offsets in the planar multifocusing case). For a central ray related to a given source/receiver pair (S_0, G_0), the

moveout can be expressed as $\Delta T = \Theta(S, G) - \Theta(S_0, G_0)$. The points S_0 and G_0 do not need to coincide, hence the central ray is not restricted to being a normal ray (finite-offset case; note that β, R_N, R_{NIP} are still related to the zero-offset ray). Once a central ray has been selected, σ plays again the role of the focusing of two notional waves (as displayed in Fig. 1 for a normal ray) and can be used to classify special data configurations (e.g., common-offset, common-source, common-receiver gathers). The spherical formula has two limiting cases for which it is equally valid: the planar reflector $R_N \to \infty$ and the point diffractor $R_N \to R_{NIP}$. As in the case of planar multifocusing, the spherical moveout formula is exact for the case it is designed for and approximate for other cases. Here, we argue that even in the approximate cases the spherical formula is robust and regular for the full offset range. The multifocusing parameter estimation procedure using the spherical moveout formula is very similar to the planar multifocusing procedure. Again, for each selected CMP location and T_0, an optimal triplet of parameters (β, R_N, R_{NIP}) is sought, such that the semblance of the prestack data from a collection of neighbouring CMP gathers along the surface $\Theta(S, G)$ (6) is maximal.

We have not fully explored the traveltime moveout expressions for other classes of curved reflectors. To our knowledge, closed expressions are available for the reflection traveltime on quadratic reflectors (ellipse, parabola, hyperbola, see Salmon (1965)) but not for higher-order polynomial reflectors. Fomel (2003) and Fomel and Kazinnik (2009) presented the reflection traveltime on a vertically oriented hyperbola. Nevertheless, the spherical reflector is an exceptional case, since it is the only reflector with finite and constant multifocusing parameters (β, R_N, R_{NIP}), and it allows the response of small bodies to be modelled $(R_N \to R_{NIP})$.

SPHERICAL MULTIFOCUSING IN THREE DIMENSIONS

The spherical multifocusing moveout formula allows a straightforward generalization to three-dimensional geometries. This is easily seen by considering Fig. 4 and using Snell's law, saying that the incident and reflected rays are coplanar with the reflector normal. Therefore, for a constant model, the centre of the sphere M, the reflection point R and the source and receiver points S and G are situated in one plane. In this plane the two-dimensional spherical moveout formula $\Theta(S, G, v_0, \beta, R_N, R_{NIP})$ (6) applies again. For the construction in Fig. 4, it is assumed that the central point X_0 is collinear with S and G but this is non-essential. The inclination ϕ of the plane containing S, G, M and R with respect to the vertical is an additional parameter. The result is a moveout formula with four parameters: $\beta, \phi, R_N, R_{NIP}$. The angles β and ϕ depend on the dip and azimuth of the reflector, R_{NIP} on its depth (distance R-X_0) and R_N on its curvature. As a by-product the multifocusing quantities σ, R^+, R^- can be obtained. The four parameter spherical moveout formula is exact for spherical bodies of arbitrary location and radius of curvature in a constant velocity model, including limiting cases such as point scatterers and plane reflectors. It applies for arbitrary source/receiver positions and is therefore valid for general topography and a wide range of offsets. It is approximate for bodies with varying curvature and an inhomogeneous overburden.

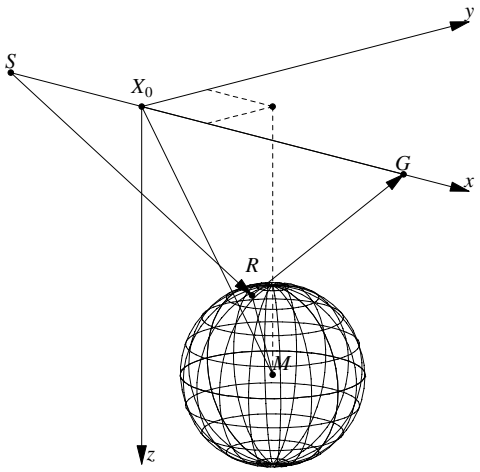

Figure 4 Spherical multifocusing in three dimensions. S, R, M and G are situated in one plane.

The four parameter moveout formula for arbitrary spherical bodies has great potential in three-dimensional seismic processing and interpretation. Many reflectors can be accurately approximated locally by spherical bodies. The limitation is that only one curvature is allowed to model their shape. Replacing the sphere by a general ellipsoid with arbitrary orientation and three radii of curvature allows more realistic and accurate moveout formulae (it leads to the problem of tangency of two three-dimensional ellipsoids studied in collision detection (Choi *et al.* 2003)) but increases the number of parameters to eight (three half axes to define the shape of the ellipsoid, three coordinates for its location and two angles for its orientation). The fact that only four parameters are needed to model reflections from spherical bodies makes the spherical multifocusing parameter estimation faster by orders of magnitude than the formulae for general ellipsoids.

COMMON REFLECTION SURFACE STACK

The common reflection surface stack (CRS) (Jäger *et al.* 2001) considers a Taylor expansion of the squared traveltime moveout T^2 (x_m, h) as a function of the common midpoint (CMP) location $x_m = \frac{1}{2}(x_G + x_S)$ and half-offset $h = \frac{1}{2}(x_G - x_S)$, around a central CMP location x_0. Because of the reciprocity of source and receiver locations, $T(x_m, h)$ is symmetric in h so odd terms in h vanish. The resulting expression to second order is very simple:

$$T^2(x_m, h) = (T_0 + A(x_m - x_0))^2 + B(x_m - x_0)^2 + Ch^2 + O((x_m - x_0)^3, h^4). \quad (7)$$

By using dynamic ray theory, the coefficients A, B and C are related to β, R_N, R_{NIP} as follows (Hubral 1983; Tygel and Santos 2007):

$$A = \frac{2\sin\beta}{v_0},\ B = \frac{2T_0\cos^2\beta}{v_0 R_N},\ C = \frac{2T_0\cos^2\beta}{v_0 R_{NIP}}. \quad (8)$$

The near-surface velocity v_0 is assumed known and locally constant. A fourth-order expansion is presented in Höcht *et al.* (1999), as well as an implicit expression for the reflection traveltime on a spherical reflector, from which approximate explicit CRS expressions are derived again by Taylor expansion. The CRS expansion gives a good approximation for the traveltime moveout, as long as it is smooth and has negligible higher-order terms, or, equivalently, for small offsets h and small $|x_m - x_0|$. These criteria are intrinsic to the Taylor expansion and not directly related to the kinematics of wave propagation. Since for each fixed x_m the moveout is hyperbolic in h, the CRS expansion (7) is strictly exact only for the case of a planar (dipping) reflector and a constant velocity overburden. In fact, there exists no model with a curved reflector for which the CRS formula is correct (Landa 2007). Even more, since both the planar and spherical multifocusing formulae deal with hyperbolic moveout as special cases, it may be argued that CRS is a limiting case of planar and spherical multifocusing. Any travel-time moveout which is fit by the CRS formula, will therefore be fit at least as well by multifocusing formulae, and, as we demonstrate in the examples below, increasingly better by MF for increasing reflector curvature. Extensions of the CRS formula to three dimensions are straightforward and have been published and implemented (Bergler *et al.* 2002; Tygel and Santos 2007).

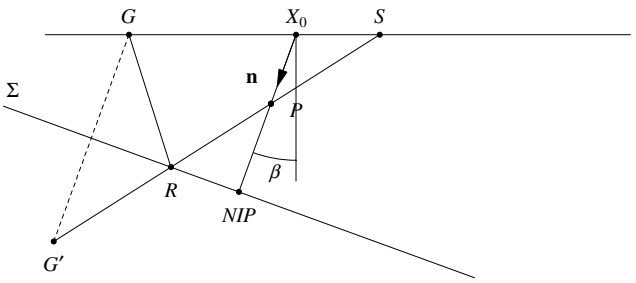

Figure 5 Geometrical derivation of planar formula for σ (see Appendix B).

EXAMPLES AND IMPLICATIONS FOR PRACTICAL INTERPRETATION

We first compare the common-reflection surface (CRS) stack, the multifocusing (MF) stack with planar and spherical expression for σ for three important cases, where the spherical expression is exact: a horizontal gently curved spherical reflector, a strongly curved spherical reflector and the limit to a point diffractor (Fig 6–8, respectively). The velocity is constant and equal to 2.0 km/s. In each example, we modelled 21 CMP's ranging from $x = -1.5$– 2 km, each with 15 (half-)offsets ranging from $h = 0$–1 km. The MF/CRS parameters for the gently curved reflector are given by $(\beta, R_N, R_{NIP}) = (10^\circ, 25\text{ km}, 1\text{ km})$ (Fig. 6), for the strongly curved reflector by $(\beta, R_N, R_{NIP}) = (0^\circ, 2\text{ km}, 1\text{ km})$ (Fig. 7) and for the limit to the point diffractor by $(\beta, R_N, R_{NIP}) = (0^\circ, 1.01\text{ km}, 1\text{ km})$ (Fig. 8). For each case, the spherical multifocusing is exact and serves as a reference.

In each case, we show the moveout surfaces (Figs 6b, 7b and 8b, respectively) for the CRS (green), planar MF (red) and spherical MF (blue). The errors, or differences with the (exact) spherical MF moveout, are shown in Figs 6(c), 7(c) and 8(c), respectively, in green for CRS and red for planar MF. Root-mean-square values of the traveltime errors are tabulated in Table 1. We see that even for the strongly curved reflector the planar MF formula gives a good approximation to the exact spherical moveout. The CRS formula however becomes increasingly inaccurate with increasing curvature.

These examples show which errors can occur for a typical multicoverage data set with offset and CMP ranges as used in the examples and assuming an effective velocity of 2km/s above a target reflector at a depth of 1 km. For a typical signal with a dominant frequency of 25 Hz, traveltime errors of 0.04 s imply that a signal cycle is missed. Stacking over more general traveltime surfaces results in a better (more coherent) stacked section, so the tests such as presented here allow to

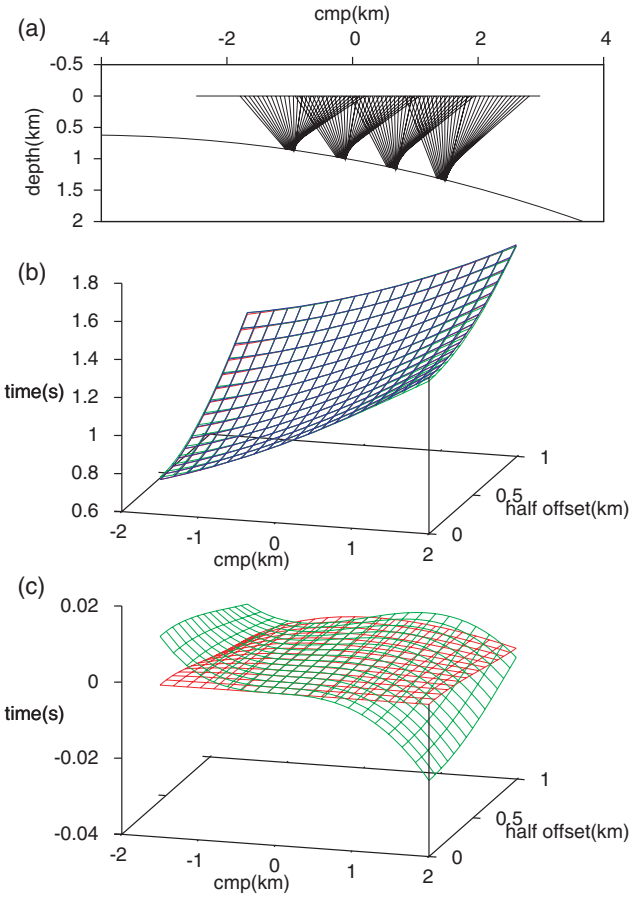

Figure 6 Gently curved reflector. a) Ray geometry (only every fifth CMP is shown). b) Moveout surfaces: common-reflection surface CRS (green), planar multifocusing (red), spherical multifocusing (blue). The spherical multifocusing expression is exact for this case. Note that the planar multifocusing moveout coincides almost completely with the spherical multifocusing move-out. c) Moveout errors: CRS (green), planar multifocusing (red).

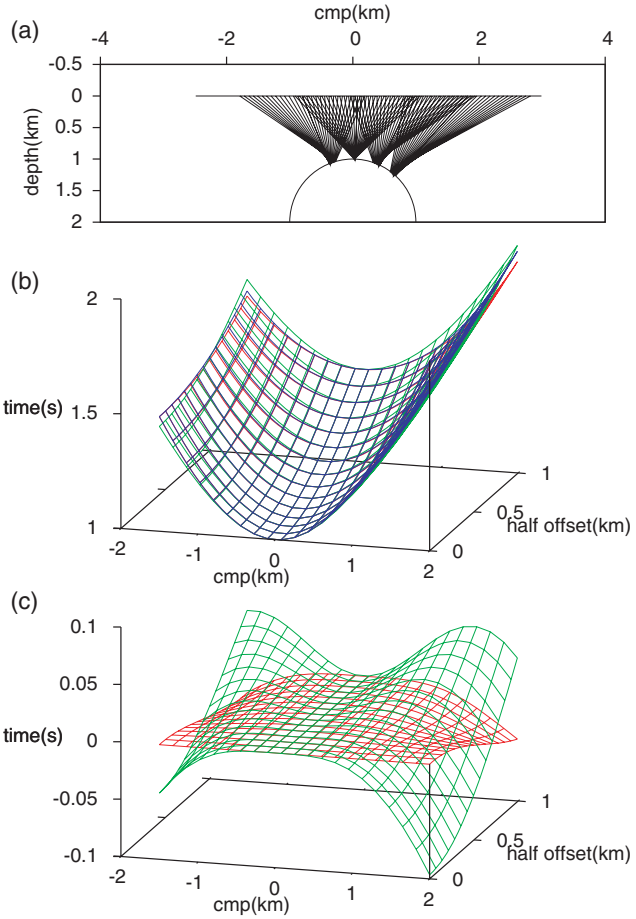

Figure 7 Strongly curved reflector. a) Ray geometry (only every fifth CMP is shown). b) Moveout surfaces: common-reflection surface CRS (green), planar multifocusing (red), spherical multifocusing (blue). The spherical multifocusing expression is exact for this case. c) Moveout errors: CRS (green), planar multifocusing (red).

assess and predict the quality of the stack obtained with the various moveout expressions discussed.

The curvature of the reflector in the second example (Fig. 7) is typical for moderately to strongly complicated structural environments (synclines, salt-dome structures, hydrocarbon reservoirs). For stronger curvatures (Fig. 8), where the differences between CRS and MF are even more pronounced, we are dealing with small scattering objects and diffracting edges, whose importance for structural interpretation has been pointed out in many publications (e.g., Khaidukov, Landa and Moser 2004).

To further support these findings, we add two examples where no analytical reflection traveltime is available: a one-layer model with a curved reflector and a multilayer model (Figs 9 and 10). Both models have a constant first layer with $v_0 = 2.0$ km/s. The deeper layers of the multilayer model are smoothly inhomogeneous, with average velocities of 2.49 km/s, 2.94 km/s, and 3.54 km/s for the second, third and fourth layer, respectively. We consider primary reflections on the first interface in the one-layer model and on the third interface in the multilayer model. In the two models, we computed rays and traveltimes by two-point raytracing for 51 CMP's ranging from 4–5 km, each with 48 (half-)offsets ranging from 0–2.35 km. In addition, we computed β, R_N and R_{NIP}(R_N and R_{NIP} using paraxial raytracing, see Moser and Červený 2007) for the zero offset (normal) ray to $x_0 = 4$ km, which we take as the central ray. We consider the traveltimes, emergence angles and radii of curvature computed by ray theory as exact for our purposes. In both models, we used the

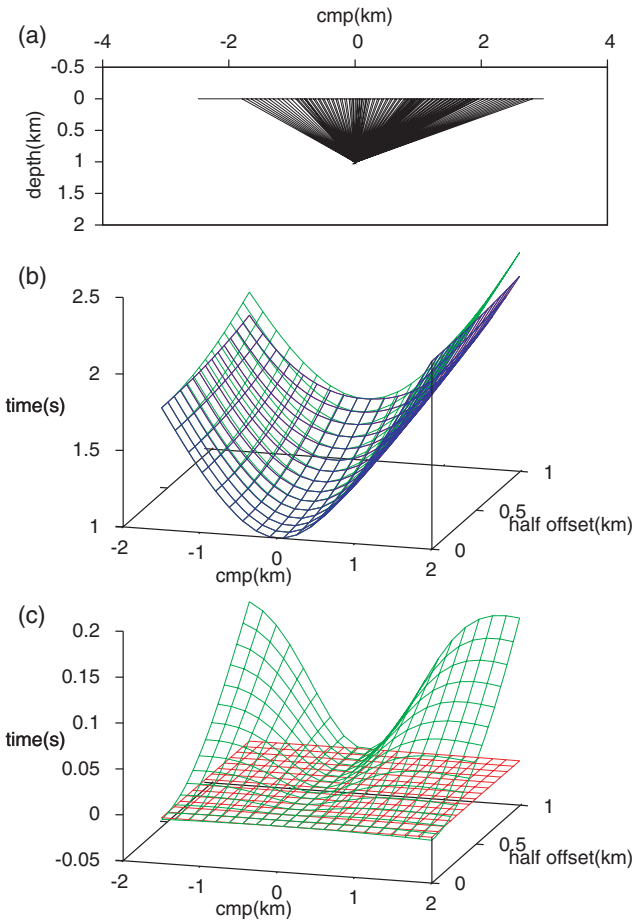

Figure 8 Limit to point diffractor. a) Ray geometry (only every fifth CMP is shown). b) Moveout surfaces: common-reflection surface CRS (green), planar multifocusing (red), spherical multifocusing (blue). The spherical multifocusing expression is exact for this case. c) Moveout errors: CRS (green), planar multifocusing (red).

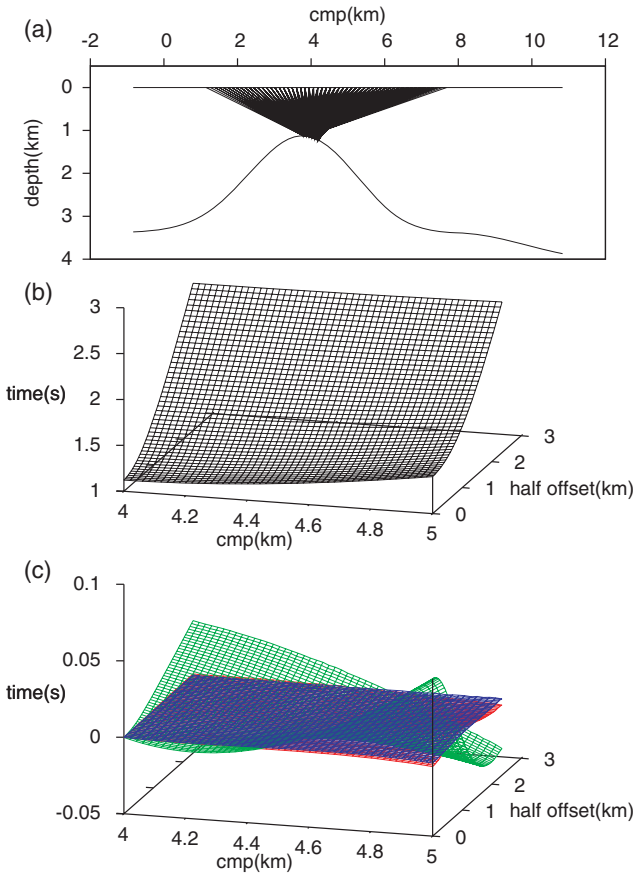

Figure 9 One-layer model with curved reflector. a) Ray geometry (only every tenth CMP and second offset is shown). b) Moveout surface from ray tracing. c) Moveout errors: CRS (green), planar multifocusing (red), spherical multifocusing (blue).

ray-based traveltimes as input data for a least-squares fitting of traveltime moveout curves, for the CRS, the planar and spherical MF expressions, respectively. The results are summarized inTables 2 and 3 and Figs 9 and 10. The misfits tabulated in the last column are the root-mean-squares of the traveltime errors over all computed rays. In both models, multifocusing is accurate within the typical sampling interval of 4 ms and has generally more accurate estimated parameters β, R_N and R_{NIP}.

DISCUSSION AND CONCLUSIONS

The insights and evidence presented in this paper allow one to take a new view on multicoverage traveltime moveout. Current methods can be broadly classified into two categories:

Table 1 RMS travel-time errors for CRS and planar MF in the examples of Figs 6–8

	CRS error (ms)	planar MF error (ms)
Gently curved reflector (Fig. 6)	5.485	1.770
Strongly curved reflector (Fig. 7)	24.700	9.560
Limit to point diffractor (Fig. 8)	51.525	0.152

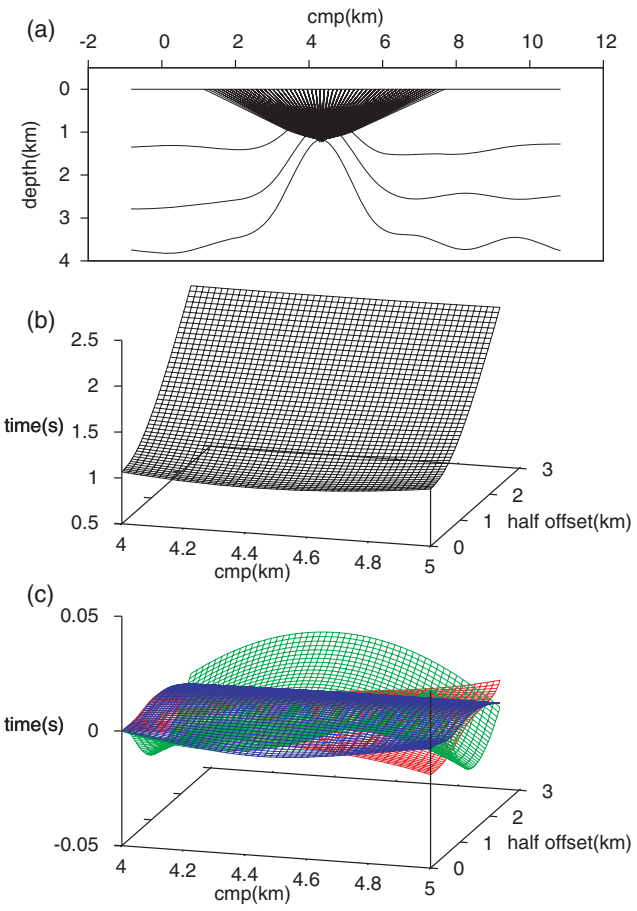

Figure 10 Multilayered model. a) Ray geometry (only every tenth CMP and second offset is shown). b) Moveout surface from ray-tracing. c) Moveout errors: CRS (green), planar multifocusing (red), spherical multifocusing (blue).

Table 2 Parameter estimation and traveltime moveout fit for CRS, planar and spherical MF in the one-layer model of Fig. 9. The misfit is the RMS of traveltime moveout errors over all rays

One-layer (Fig. 9)	β (deg)	R_N (km)	R_{NIP} (km)	misfit (ms)
exact	1.60	1.738	1.141	
CRS	4.87	3.028	1.154	15.79
MF planar	2.05	1.833	1.125	1.24
MF spherical	2.00	1.850	1.123	0.32

Taylor expansion methods and methods based on the kinematics of wave propagation. The common-reflection surface (CRS) stack method belongs to the first class, has been subject of many publications and is widely used now. In its current form, it is essentially a quadratic moveout formula (Tygel and Santos 2007), although in principle higher-order terms in the Taylor expansion may be considered. Thanks to relatively simple algebra, extensions to three dimensions have been available already for a long time. The multifocusing method belongs to the class of methods based on the kinematics of wave propagation and has been designed to approximate the response at the source and receiver points by two spherical waves. These two spherical waves are mutually related by the focusing quantity σ. We emphasize the character of the focusing quantity and make clear that it is a parameter function, rather than a parameter itself. The σ-function can be designed to be exact in generic cases. The complexity of the algebra has prevented the exploration of general classes of reflectors and the extension of multifocusing to three dimensions but one such generic case in two dimensions has been known for a long time: the plane reflector.

Table 3 Parameter estimation and traveltime moveout fit for CRS, planar and spherical MF in the multi-layer model of Fig. 10. The misfit is the RMS of traveltime moveout errors over all rays

Multi layer (Fig. 10)	β (deg)	R_N (km)	R_{NIP} (km)	misfit (ms)
exact	18.47	1.323	1.345	
CRS	16.69	1.644	1.132	9.18
MF planar	19.25	1.259	1.272	3.55
MF spherical	17.26	1.419	1.285	2.86

In this paper, we investigate the σ-function for a wider class of reflectors: the spherical reflector. In the derivation of the spherical multifocusing moveout it turns out that the expression for traveltime moveout is easier to obtain than an expression for σ. The reflection traveltime on a spherical reflector has a long history in various disguises (Alhazen's problem, optical reflection on a spherical mirror, the circular billiard, or collision detection in robotics). The resulting equation is a fourth-order algebraic equation, for which analytical solutions are available (four complex-valued solutions in general). The reflection traveltime and reflection point can be obtained directly from the solutions, the multifocusing quantities σ, R^+ and R^- as a by-product. The spherical moveout is therefore firmly embedded in the general multifocusing technique and its theory (Gelchinsky *et al.* 1999a,b). At the same time, it simplifies and generalizes multifocusing. In this sense, the situation is similar to the well-known analogy of Wittgenstein's ladder (Scruton 2001). One needs a ladder to reach a higher point of view, in order to realize that one no longer needs the ladder.

The spherical multifocusing expression is unconditionally robust (no singularities as in the planar case), applies without modification for any central ray (zero- as well as finite-offset, stacked common-offset sections can be generated without additional effort), to general topography on rugged surfaces and it allows a straightforward extension to three dimensions. In two dimensions, it needs the same triplet of parameters as the common-reflection surface stack and planar multifocusing methods: β, R_N, R_{NIP}. In three dimensions, it needs only one additional parameter: the inclination of the plane containing the source and receiver point and centre of the spherical reflector – four parameters in total. We argue that the three-dimensional spherical multifocusing can be of great practical use, since it uses only four parameters (compared to up to eight for other methods) and the modeling of three-dimensional reflecting bodies by spheres of arbitrary size and location allows for a considerable generality in three-dimensional structural interpretation.

We believe that multifocusing has the potential to open up a way to search for different geometrical bodies, such as general three-dimensional ellipsoids, paraboloids and an extension of the class of generic cases is certainly feasible. Also, we believe that overburden inhomogeneity and anisotropy (transverse isotropy) can be addressed via an extension of the framework presented here. Nevertheless, the spherical multifocusing has the advantage that it applies to geometries with finite and constant β, R_N, R_{NIP}, and therefore has the potential to combine generality and simplicity, as well as computational efficiency in the parameter estimation. The multifocusing generic cases and the spherical reflector in particular, allow a prestack seismic data volume to be decomposed into responses from elementary curved reflector segments. They therefore act as templates of seismic reflection response. Even more, we show that the spherical multifocusing is not restricted to reflection response but applies to the response from strongly curved reflectors as well and to limiting cases such as point diffractors. By contrast, our numerical examples show that, while the planar multifocusing is remarkably accurate in many cases, the common-reflection surface stack method is not good for diffractions. The reason for this is, as we argue, that the CRS moveout is essentially a quadratic expression (a hyperbolic Taylor expansion), whereas the multifocusing moveout is a double square-root expression. The importance of diffractions for the interpretation of small-scale structural elements, especially in reservoir imaging has been pointed out in several recent publications (e.g., Khaidukov *et al.* 2004).

ACKNOWLEDGEMENTS

The first author, E. Landa, would like to thank Total for supporting this research. OPERA is a private organization funded by Total whose main objective is to carry out applied research in petroleum geophysics. The second author, S. Keydar, is grateful to the Geophysical Institute of Israel for permission to publish this paper. For various derivations we have used the Maxima computer algebra system (http://maxima.sourceforge.net/). We are grateful to the reviewers for their many useful comments.

REFERENCES

Alkhalifah T. and Tsvankin I. 1995. Velocity analysis for tranversely isotropic media. *Geophysics* **60**, 1550–1566.

de Bazelaire E. 1988. Normal moveout correction revisited: inhomogeneous media and curved interfaces. *Geophysics* **53**, 143–157.

Bergler S., Hubral P., Marchetti P., Cristini A. and Cardone G. 2002. 3D common-reflection-surface stack and kinematic wavefield attributes. *The Leading Edge* **21**, 1010.

Berkovich A., Belfer I. and Landa E. 2008, Multifocusing as a method of improving subsurface imaging. *The Leading Edge* **27**, 250–257.

Burnside W.S. and Panton A.W. 1960. *The Theory of Equations With an Introduction To The Theory of Binary Algebraic Forms*. Dover, New York.

Castle R. 1994. A theory of normal moveout. *Geophysics* **59**, 983–999.

Causse E., Hangen G.U. and Rommel B. 2000. Large-offset approximation to seismic reflection traveltimes. *Geophysical Prospecting* **48**, 763–778.

Causse E. 2002. Seismic traveltime approximations with high accuracy at all offsets. 64th EAGE meeting, Florence, Italy, Extended Abstracts.

Červený V. 2001. *Seismic Ray Theory*. Cambridge University Press.

Choi Y.K., Wang W. and Kim M.S. 2003. Exact collision detection of two moving ellipsoids under rational motions. *Proceedings IEEE International Conference on Robotics and Automation* **1**, 349–354.

Dörrie H. 1965. *100 Great Problems of Elementary Mathematics: Their History and Solutions*. Dover, New York.

Drexler M. and Gander M.J. 1998. Circular billiard. *SIAM Review* **40**, 315–323.

Eisenberg-Klein G., Prüssmann J., Gierse G. and Trappe H. 2008. Noise reduction in 2D and 3D seismic imaging by the CRS method. *The Leading Edge* **27**, 258–265.

Fomel S. 2003. Theory of differential offset continuation. *Geophysics* **68**, 718–732.

Fomel S. and Kazinnik R. 2009. Non-hyperbolic common reflection surface. 79th SEG meeting, Houston, Texas, USA, Extended Abstracts.

Gelchinsky B., Berkovitch A. and Keydar S. 1999a. Multifocusing homeomorphic imaging – Part 1. Basic concepts and formulae. *Journal of Applied Geophysics* **42**, 229–242.

Gelchinsky B., Berkovitch A. and Keydar S. 1999b. Multifocusing homeomorphic imaging – Part 2. Multifold data set and multifocusing. *Journal of Applied Geophysics* **42**, 243–260.

Gurevich B., Keydar S. and Landa E. 2002. Multifocusing imaging over an irregular topography. *Geophysics* **67**, 639–643.

Höcht G., de Bazelaire E., Majer P. and Hubral P. 1999. Seismics and optics: hyperbolae and curvatures. *Journal of Applied Geophysics* **42**, 261–281.

Hubral P. 1983. Computing true amplitude reflections in a laterally inhomogeneous earth. *Geophysics* **48**, 1051–1062.

Hubral P. 1999. Macro model independent seismic reflection imaging. *Journal of Applied Geophysics* **42**, 3–4.

Jäger R., Mann J., Höcht G. and Hubral P. 2001. Common-reflecting-surface stack: Image and attributes. *Geophysics* **66**, 97–109.

Khaidukov V., Landa E. and Moser T.J. 2004. Diffraction imaging by focusing-defocusing: An outlook on seismic superresolution. *Geophysics* **69**, 1478–1490.

Landa E. 2007. *Beyond Conventional Seismic Imaging*. EAGE.

Landa E., Gurevich B., Keydar S. and Trachtman P. 1999. Application of multifocusing method for subsurface imaging. *Journal of Applied Geophysics* **42**, 283–300.

Malovichko A.A. 1978. A new representation of the travel time curve of reflected waves in horizontally layered media. *Applied Geophysics* **91**, 47–53 (in Russian).

Mann J., Jäger R., Müller T., Höcht G. and Hubral P. 1999. Common-reflection-surface stack a real data example. *Journal of Applied Geophysics* **42**, 301–318.

May B.T. and Straley D.K. 1979. Higher-order moveout spectra. *Geophysics* **44**, 1193–1207.

Moser T.J. and Červený V. 2007. Paraxial ray methods in anisotropic inhomogeneous media. *Geophysical Prospecting* **55**, 21–37.

Neumann P.M. 1998. Reflections on reflection in a spherical mirror. *American Mathematical Monthly* **105**, 523–528.

Salmon G. 1960. *Conic Sections*, 6th edn. Chelsea, New York.

Scruton R. 2001. *Short History of Modern Philosophy*. Routledge.

Sword C.H. 1987. A Soviet look at datum shift. SEP-51, Stanford Exploration Project, 313–316.

Taner M.T. and Koehler F. 1969. Velocity spectra digital computer derivation and applications of velocity functions. *Geophysics* **34**, 859–881.

Taner M.T., Treitel S., Al-Chalabi M. and Fomel S. 2007. An offset dependent NMO velocity model. 69th EAGE meeting, London, UK, Extended Abstracts.

Tygel M., Santos L.T. and Schleicher J. 1999. Multifocus moveout revisited: derivations and alternative expressions. *Journal of Applied Geophysics* **42**, 319–331.

Tygel M. and Santos L.T. 2007. Quadratic normal moveouts of symmetric reflections in elastic media: A quick tutorial. *Studia Geophysica et Geodætica* **51**, 185–206.

APPENDIX A: RELATION OF WAVEFRONT CURVATURES AND FOCUSING QUANTITY

We consider solutions of the dynamic ray-tracing equations in a two-dimensional isotropic medium, for a ray parametrized by traveltime t, connecting two end points at the surface given by $\Delta X^+ = x_S - x_0$ and $\Delta X^- = x_G - x_0$ and reflecting once on a subsurface reflector (see Fig. 1a). In this geometry, the ray is planar and the dynamic ray tracing equations can be decoupled into an in-plane and transverse system. The solutions to the in-plane system can be characterized by scalar functions $Q(t)$ and $P(t)$, where $Q(t)$ is the derivative of the ray position perpendicularly to the ray and $P(t)$ the derivative of the corresponding component of the slowness vector, both with respect to an initial ray parameter, which we do not need to specify here (see Červený 2001, section 4.13.1 for details). The wavefront curvature along the ray is given by the relation $k(t) = V(t)\,P(t)/Q(t)$, where $V(t)$ is the propagation velocity. Any solution $Q(t)$, $P(t)$ to the dynamic ray equations can be written as a linear combination of two independent solutions $Q_1(t)$, $P_1(t)$ and $Q_2(t)$, $P_2(t)$:

$$Q(t) = a\,Q_1(t) + b\,Q_2(t),\; P(t) = a\,P_1(t) + b\,P_2(t). \tag{9}$$

We choose two special solutions $Q_1(t)$ and $Q_2(t)$ such that

$$Q_1^+ = Q_1^- = Q_2^+ = -Q_2^- = 1, \tag{10}$$

where superscripts $^\pm$ denote evaluations at the ray end points $t^\pm$. From geometrical considerations, it follows that Q_1 corresponds to the N-wave (its ray position derivative has equal signs at t^- and t^+), and Q_2 to the NIP-wave (its ray position derivative has opposite signs). For an arbitrary solution we take the normalization $Q^+ = 1$ and obtain

$$Q^+ = a + b = 1,\; Q^- = a - b = 1 - 2b. \tag{11}$$

The wavefront curvature at the ray end points is then given by

$$k^\pm = V^\pm \frac{a\,P_1^\pm + b\,P_2^\pm}{a\,Q_1^\pm + b\,Q_2^\pm}. \tag{12}$$

Dividing by $aQ_1^\pm$, and defining the focusing quantity $\sigma = b/a$ we obtain

$$k^\pm = \frac{k_1^\pm \pm \sigma k_2^\pm}{1 \pm \sigma} \tag{13}$$

Defining radii of wavefront curvature $R^\pm = 1/k^\pm$ and identifying $k_1^\pm, k_2^\pm$ with $1/R_N$ and $1/R_{NIP}$, respectively, this results in (2).

It remains to find an expression for $\sigma = b/a = b/(1-b)$. Since, by definition, Q is the perpendicular displacement to

the ray, we have at the ray end points

$$\frac{\Delta X^-}{\Delta X^+} = \frac{Q^- \cos\beta^+}{Q^+ \cos\beta^-}, \tag{14}$$

where $\beta^\pm$ are the emergence angles at the ray end points (note that in some publications the notation β_0 is used for the emergence angle β at the central point x_0 used in this paper). From (11), we have a relation between ΔX^- and ΔX^+ in terms of σ:

$$\frac{\Delta X^-}{\Delta X^+} = \frac{\cos\beta^+(1-\sigma)}{\cos\beta^-(1+\sigma)} \tag{15}$$

For a wave arriving at $\pm$ we have

$$\frac{\mathrm{d}T}{\mathrm{d}\Delta X^\pm} = \frac{\sin\beta^\pm}{v_0}. \tag{16}$$

Differentiating the multifocusing travel-time moveout (1) with respect to ΔX^+ and ΔX^-, respectively, we obtain:

$$\frac{\mathrm{d}T}{\mathrm{d}\Delta X^\pm} = \frac{\Delta X^\pm + R^\pm \sin\beta}{v_0\sqrt{(\Delta X^\pm)^2 + 2R^\pm \Delta X^\pm \sin\beta + (R^\pm)^2}}. \tag{17}$$

Here, we assume that $R^\pm$ are locally constant. Solving $\beta^\pm$ from (16) and (17) we obtain

$$\frac{\Delta X^-}{\Delta X^+} = \frac{R^+(1-\sigma)}{R^-(1+\sigma)}\sqrt{\frac{(\Delta X^-)^2 + 2R^-\Delta X^- \sin\beta + (R^-)^2}{(\Delta X^+)^2 + 2R^+\Delta X^+ \sin\beta + (R^+)^2}} \tag{18}$$

Inserting (13) in (18), solving for σ, expanding in powers of $k_N = 1/R_N$ and retaining the leading term gives (4).

We note that the expression (4) appears sometimes with a $-$sign in front of the term containing $\sin\beta$, depending on whether β is defined clockwise or counterclockwise. Also, taking the same expression for $-\sigma$ is equivalent to σ with S and G exchanged, thanks to reciprocity. The expression for planar σ given in Tygel *et al.* (1999) is incorrect, according to three independent derivations leading to (4) given in this Appendix, in Appendix B and in Landa *et al.* (1999).

APPENDIX B: FOCUSING QUANTITY FOR A PLANE DIPPING REFLECTOR

We define $\mathbf{x}_0 = (x_0, z_0), \mathbf{x}_G = (x_G, z_G), \mathbf{x}_S = (x_S, z_S)$ and $\mathbf{n} = (\sin\beta, \cos\beta)$ (see Fig. 5). The NIP ray is given by $\mathbf{x} = \mathbf{x}_0 + u\mathbf{n}$ $(0 < u < R_{NIP})$, the NIP point by $\mathbf{x}_{NIP} = \mathbf{x}_0 + R_{NIP}\mathbf{n}$ and the plane reflector Σ is defined by $(\mathbf{x} - \mathbf{x}_{NIP})^T\mathbf{n} = 0$. For a plane reflector $R_N = \infty$ and (2) gives

$$\sigma = R_{NIP}/(R^+ - R_{NIP}) \tag{19}$$

Here, R^+ is the radius of the wave Σ_S and equal to the length of the line segment $X_0 - P$. To find it, we construct the point P as follows. The mirror point G' of G in Σ is given by:

$$\mathbf{x}_{G'} = \mathbf{x}_G - 2\mathbf{n}(\mathbf{x}_G - \mathbf{x}_{NIP})^T\mathbf{n}. \tag{20}$$

The focusing P point is the intersection of $G' - S$ and $X_0 - NIP$ and satisfies

$$\det(\mathbf{x}_P - \mathbf{x}_S, \mathbf{x}_{G'} - \mathbf{x}_S) = 0, \tag{21}$$

where det is a 2×2-determinant. Substituting $\mathbf{x}_P = \mathbf{x}_0 + u_P\mathbf{n}$ in (21) and solving for u_P, we find

$$u_P = -\det(\mathbf{x}_0 - \mathbf{x}_S, \mathbf{x}_{G'} - \mathbf{x}_S)/\det(\mathbf{n}, \mathbf{x}_{G'} - \mathbf{x}_S). \tag{22}$$

For R^+ this gives $R^+ = -u_P$ and for σ:

$$\sigma = R_{NIP}/(u_P - R_{NIP}) \tag{23}$$

Expression (23) with (22) and (20) is a general expression for σ for a planar reflector and arbitrary locations for the source, receiver and central points $\mathbf{x}_S, \mathbf{x}_G, \mathbf{x}_0$. It can be used therefore for a general surface topography (Gurevich, Keydar and Landa 2002). Taking a planar topography $z_G = z_0 = z_S = 0$ and writing $\Delta X^+ = x_S - x_0$ and $\Delta X^- = x_G - x_0$, we obtain after some algebra the same expression for planar σ (4).

APPENDIX C: TRAVEL TIME ON A SPHERICAL REFLECTOR

We quote the formula for reflection on a spherical reflector (Drexler and Gander 1998), since to our knowledge it has not appeared before in the geophysical literature. The problem of finding the reflection traveltime from $\mathbf{x}_S$ to $\mathbf{x}_R$ to $\mathbf{x}_G$ can be formulated as the problem of the tangency of the ellipse E with foci $\mathbf{x}_S$ and $\mathbf{x}_G$ and the circle C (Fig. 3). For simplicity (but without loss of generality) we choose a coordinate system with $\mathbf{x}_S = (-h, 0)$ and $\mathbf{x}_G = (+h, 0)$, with the half-offset h. In a constant velocity v_0 the traveltime T satisfies the ellipse equation:

$$E = \frac{x^2}{(v_0T/2)^2} + \frac{z^2}{(v_0T/2)^2 - h^2} - 1 = 0. \tag{24}$$

The circular reflector is given by

$$C = (x - x_c)^2 + (z - z_c)^2 - r_c^2 = 0. \tag{25}$$

The tangency condition is given by

$$\det(\nabla E, \nabla C) = \frac{4x(z - z_c)}{(v_0T/2)^2} - \frac{4(x - x_c)z}{(v_0T/2)^2 - h^2} = 0. \tag{26}$$

Solving T^2 from (26) we obtain

$$(v_0T/2)^2 = \frac{h^2x(z_c - z)}{xz_c - x_cz}. \tag{27}$$

Inserting (27) in (24), writing the circle as $x = x_c + r_c \cos\theta, z = z_c + r_c \sin\theta$ and substituting $\theta = 2 \arctan u$ we get

$$\frac{Q(u)}{2h^2u(u-1)(u+1)} = 0 \tag{28}$$

where

$$Q(u) = Au^4 + 2Bu^3 + 6Cu^2 + 2Du + E$$

$$A = (x_c - r_c)z_c,\ B = -z_c^2 + x_c^2 - r_c x_c - h^2,$$
$$C = -x_c z_c,\ D = z_c^2 - x_c^2 - r_c x_c + h^2,\ E = (x_c + r_c)z_c.$$

In (28), $u = 0$ corresponds to a vertical tangent of E and C, which is only possible if $z_c = 0$. Similarly, $u = \pm 1$ corresponds to a horizontal tangent, which is possible only if $x_c = 0$. Therefore all solutions to (28) are covered by

$$Q(u) = 0. \tag{29}$$

This is a quartic equation in u, with four complex-valued solutions in general. Writing the solutions in terms of θ, we get the reflection point (x, z) from the circle equation and the reflection traveltime T from (27).